H + Ar collisions. I. Experimental charge-production cross sections*

B. Van Zyl, T. Q. Le, H. Neumann, and R. C. Amme
University of Denver, Denver, Colorado 80208
(Received 10 January 1977)

Absolute total cross sections for producing H^+, Ar^+, H^-, and e^- and the large-angle-scattering differential cross section for H^+ production have been determined for H + Ar collisions. These determinations were made by combining experimental measurements, described here, and theoretical calculations, described in the following paper. The hydrogen-atom energy range covered extends from 3 keV down to 50 eV. An interesting structured cross section is found for the $H^- + Ar^+$ ion pair formation reaction. The experimental techniques used are described and the cross sections are compared, where possible, with the data of other investigators. An interpretation of the results, based on the details of the H + Ar interaction, is suggested.

I. INTRODUCTION

The Aurora Borealis and the Aurora Australis rank among the most magnificent and scientifically interesting of all naturally occurring atmospheric phenomena. First studied by Greek philosophers as early as the sixth century B.C.,[1] the aurora today remains the subject of intensive scientific investigation. In spite of this voluminous effort, however, such important topics as the total energy input to the atmosphere and the eventual fate of this input as a function of the nature of the precipitating sponsor particles are not yet well characterized. The discovery of atomic hydrogen line emissions in the auroral spectrum by Vegard[2] in 1939, and his subsequent finding that these features exhibited Doppler-shifted profiles,[3] constituted direct evidence that fast hydrogen particles contributed to auroral phenomena. Even though the vivid optical displays normally associated with an aurora were soon attributed to precipitating electrons, the so-called proton aurora is important in its own right, in that this diffuse phenomenon results in a total energy deposition into the atomsphere of approximately the same magnitude as the more localized electron-sponsored occurrences.[4]

It was predicted by Bates[5] that a proton incident on the atmosphere at auroral altitudes (typically 100 to 300 km) should spend a large fraction of its time as a neutral hydrogen atom because of charge-transfer processes. Implicit in this reasoning is the fact that the net atmospheric charge-transfer efficiency is larger than its reverse counterpart, i.e., the net ionization-stripping efficiency for turning a hydrogen atom back into a proton. This is certainly true in the energy range below 5 keV, an important energy range in the aurora. The importance of this lower energy regime is brought out by measurements of the energy spectra of precipitating hydrogen particles in an aurora, as reviewed by McNeal and Birely.[6] These authors also stress the importance of the neutral-hydrogen-atom component of the incident flux at lower energies. These observations, coupled with the fact that all incident particles, independent of their initial energy, must pass through the lower energy regime on their route to eventual thermalization, enhance the need for cross sections for auroral processes at the lower energies.

In order to quantitatively compare the net effectiveness of H^+ and H in sponsoring various auroral phenomena at these lower energies, their equilibrium charge-state fractions must be known. This requires a knowledge of the charge-transfer cross sections σ_{10} and the reverse ionization-stripping cross sections σ_{01} for all the important atmospheric gas species. Numerous measurements of the σ_{10} cross sections are available,[7] fulfilling this half of the requirement. On the other hand, the σ_{01} data are meager, with only one recent set of measurements[8] extending to below 1 keV hydrogen-atom energy.

To satisfy this need, an experimental program was mounted to measure various cross sections for charged-particle production for 50-eV to 3-keV hydrogen-atom collisions with N_2, O_2, Ar, He, and H_2 targets. For Ar targets, three types of reactions can lead to charged collision products. These are

$$H + Ar \rightarrow H^+ + e^- + Ar, \quad (1)$$

$$H + Ar \rightarrow H + e^- + Ar^+, \quad (2)$$

$$H + Ar \rightarrow H^- + Ar^+, \quad (3)$$

where multiple ionization phenomena have been ignored.[9] The σ_{01} cross section is, of course, that defined by reaction (1), reaction (3) defines σ_{0-1}. The Ar^+ formation cross section σ_{Ar^+} represents the sum of the cross sections for reactions (2) and (3). Finally, the total negative charge production cross section σ_t^- is the sum of the cross sections

for all three processes, and must obviously be identical with σ_t^+, the cross section for total positive charge production. Nevertheless, the distinction is here made, as these total charge production cross sections have been individually measured.

The technique used to determine the σ_{01} cross section stems from the procedure employed by McNeal and Clark[10] for making similar measurements for $H+N_2$ collisions above 1 keV. The technique involves measuring σ_t^- and σ_{Ar^+} independently and determining σ_{01} from the relationship:

$$\sigma_{01}=\sigma_t^- - \sigma_{Ar^+}. \tag{4}$$

Preliminary measurements, however, soon revealed that the σ_{Ar^+} measurement was fraught with difficulty. Fast protons arising from reaction (1) and scattered to large angles during their formation were found to be contributing to the measured slow Ar^+ ion signal. The problem became increasingly severe as the hydrogen-atom energy was extended into the range below 1 keV.

It was found necessary to employ a combination of experimental measurements and theoretical scattering calculations to resolve this difficulty and to extract the desired cross-section values. While the procedures used are laborious, they do result in rather complete data describing all charge production channels available to the post-collision products. The experimental measurements and the techniques applied for their accomplishment are described here, and the total cross sections for H^+, Ar^+, H^-, and e^- are presented. The differential cross section for H^+ production and the theoretical scattering calculations allowing its determination are described in the following paper (paper II).

We have selected $H+Ar$ collisions as a topic for this first paper for a number of reasons. First, the Ar target species, being an atomic system, facilitated the theoretical scattering calculations required for interpretation of the experimental measurements. Second, the angular scattering of the product H^+ was both predicted and found to be large from this massive, high-Z target, making it an obvious candidate for early exploration. Third, the interesting structure evident in the H^-+Ar^+ ion pair formation cross section warrants attention over and above application of these results to understanding auroral phenomena. Finally, the sheer volume of material requiring presentation in order to justify the many new techniques employed here prohibits consideration of more than one collision type. However, the various test data presented to establish the validity of the method include results for other target species in order that such data will not need to be detailed in subsequent publications.

II. BASIC EXPERIMENTAL PROCEDURE

Consider a narrow parallel beam of hydrogen atoms of flux B (in atoms/sec) traversing a region containing Ar atoms at density N (in atoms/cm^3). Assume that a suitable detector can measure a signal S_m (in ions/sec) produced along a beam path length L (in cm), from a process having cross section σ_m (in cm^2). These parameters are related by the expression

$$S_m = BNL\sigma_m. \tag{5}$$

Thus to determine the cross section σ_m, the other factors in Eq. (5) must be measured or otherwise determined. The procedures used to generate and absolutely determine the magnitudes of B and N are presented here. Those for determining S_m will be considered in Sec. III.

The technique used in this work for generating the fast neutral hydrogen-atom beam consists of photodetaching electrons from negative hydrogen ions H^-. The H^- ions, formed in a duoplasmatron source, are extracted, mass-analyzed, and focused into a parallel or slightly converging beam having a diameter on the order of 1 mm.[11] This beam is then directed through the cavity of a YAlG laser (1064 nm) whose end mirrors are totally reflecting. The photodetachment reaction, i.e.,

$$H^- + h\nu \rightarrow H + e^-, \tag{6}$$

proceeds with such efficiency that several percent of the primary H^- ions are neutralized in the energy range of interest.[12] The remaining emergent H^- ions are then electrostatically swept from the beam path before the product hydrogen atoms enter the target scattering cell.

The details of this procedure are presented elsewhere[13] and will not be reviewed here. It should be noted, however, that the execution of the measurements reported here would have been difficult without a neutral beam of the quality available. For example, because the momentum transfer to the hydrogen atom during its formation is negligible, the same stringent directionality and divergence conditions imposed on the initial H^- beam are maintained in its neutral counterpart. As will be seen in the next section, having a nondivergent, directionally defined atom beam of small width is fundamental to the measurements. Having a beam whose absolute intensity can be determined to within a ±3% uncertainty[14] and an even smaller relative uncertainty facilitates an accurate comparison of various cross-section measurements made at different times under differing conditions.

The target-cell density [the N in Eq. (5)] is determined by simultaneous measurement of the target gas pressure and temperature. During the course of each cross-section measurement period, a Bayard-Alpert-type ionization gauge was used to monitor the target-cell pressure. Prior to and after each such period, this gauge was calibrated against a capacitance diaphragm manometer at a pressure comparable to that used during the cross-section measurements (typically 1 to 3×10^{-4} Torr). A sufficient number of such calibrations were made to allow the statistical variance to be ascertained.

The capacitance diaphragm manometer was in turn calibrated in the 0.1 Torr pressure region against a micrometer-point contact manometer of the type described by Ruthberg.[15] This apparatus, constructed in our laboratory, is able to measure pressure to within a ±1% uncertainty in the 0.1 Torr region.

A series of measurements over an extended time period were undertaken to demonstrate the pressure response linearity of the capacitance diaphragm manometer between about 0.1 and 10^{-4} Torr. These studies, making use of the electrostatic calibration feature of the manometer,[16] have been described elsewhere.[17] The conclusion drawn from the studies was that the manometer used has a linear response to pressure over the range cited to within an uncertainty of ±2.1%.

The various uncertainties discussed above were combined with others (e.g., temperature measurements, ionization gauge space charge nonlinearities, thermal transpiration effects, instrument zero drifts, measurement statistics, etc., for a total of 22 uncertainty sources) by quadrature addition to give a net uncertainty of ±6% for the target-cell density determination.

III. NEUTRAL SCATTERING TARGET CELL; DATA ACQUISITION AND ANALYSIS

The neutral-atom scattering target cell used for all the measurements reported here is shown schematically in Fig. 1. The energy-selected precisely collimated H-atom beam enters from the left through two 5-mm-diam differential pumping apertures coaxial with the scattering cell axis. Gas feed and pressure monitor ports are shown. The charged particle trap at the rear of the cell serves to prevent secondary ions/electrons ejected from the neutral collector surface from re-entering the gas scattering region. The Ar target gas pressure ranged from about 1 to 3×10^{-4} Torr, while the pressure in the main vacuum tank was about two orders of magnitude smaller. This large ratio kept the background neutral flux entering the cell (from background gas stripping of H^- ions in the photodetachment region) at a level of only about 10% of the photodetachment generated flux. The contributions of these background neutrals to all signal measurements were evaluated by switching off the photodetaching YAlG laser light source.

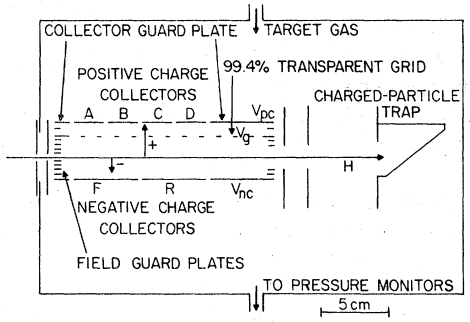

FIG. 1. Target cell and charged particle detectors.

The basic charged particle detector arrangement used is of the parallel-plate ionization-chamber type first employed by Utterback and Miller.[18] However, two important changes were made. First, the uniformity of the various charged particle collection fields within the cell is established by employing field guard plates, as shown in Fig. 1, as opposed to locating the actual signal collectors in the center of an "infinite" collector plane. This feature allows placement of the signal collectors much closer to the entrance to the target cell; thus a "starting point" for the reactions occurring within the cell can be reasonably established. Second, rather than using a single collector, arrays of such collectors are employed: two for negative charge collection and four for positive charge collection. This allows measurement of the various charged particle signals as a function of the distance into the target cell.

For collecting negatively charged particles from H+Ar collisions, the negative charge collectors are connected to an electrometer and set to zero potential (i.e., $V_{nc}=0$). The potential applied to the 99.4% transparent grid V_g is typically a few hundred volts negative, and that to V_{pc} set to $0.6V_g$. Under these conditions, electrons (contributions from negative ions will be discussed later) produced by ionizing collisions along the neutral beam path through the cell are driven to the negative charge collectors by the negative grid potential. If a fast angularly scattered proton or hydrogen atom were to impinge on one of the negative charge collector surfaces and eject a secondary electron, this electron would be "trapped" at the collector surface by the repulsion it experiences from the negative grid potential. Similarly, if such a fast

scattered particle were to impact on a positive charge collector surface, any liberated secondary electrons would also be trapped, because V_g is more negative than V_{pc}. Hence, the collection of negatively charged collision products is relatively free of erroneous contributions to the measured signals from secondary electron effects.[19]

If, on the other hand, the same procedure were followed in collecting slow positive Ar^+ ions by simply reversing all cell potentials, secondary electron effects would generate problems. Thus, if the grid potential were positive to drive slow positive ions to the collectors normally used for electrons, any secondary electrons released from the collector surfaces would readily escape under their attraction to the now positive grid potential V_g. Since a leaving electron looks identical, to the detector, to an arriving ion, an overestimate of the signal would result. Looking ahead, the authors suggest that at least some of the disagreement between the Ar^+ production cross section reported here and that reported by McNeal, Clark, and Klingberg[20] may be attributed to this problem. To check this hypothesis, measurements were made under target-cell conditions similar to those employed by these workers, and results similar to theirs were obtained.[21]

To overcome this secondary electron problem, the slow Ar^+ ions are collected at the positive charge collectors shown in Fig. 1. For these measurements, the positive charge collectors are set to zero potential ($V_{pc}=0$); typical values for V_g and V_{nc} are -15 and $+75$ V, respectively. Under these conditions, the target-cell axis lies on a plane whose potential is midway between that of the grid and the negative charge collector, i.e., at $+30$ V. Slow positive ions formed are thus accelerated toward and pass through the highly transparent grid,[22] decelerating as they approach the positive charge collectors, but still arriving with about 30 eV energy. Note, furthermore, that the grid potential is now negative with respect to all collector surfaces, thereby trapping secondary electrons as in the case of the negative charge collection measurements.

Unfortunately however, the measurement of the Ar^+ production cross section σ_{Ar^+} is afflicted with yet another problem. This difficulty is illustrated by the data shown in Fig. 2, where the measured positive ion signals to collectors A, B, C, and D (see Fig. 1) are plotted as a function of the distances of these collectors into the target cell. Similar data at energies other than 630 eV show that the disparity between the signals measured at the various collectors increases with decreasing energy, but diminishes to only a few percent at energies above about 2 keV.

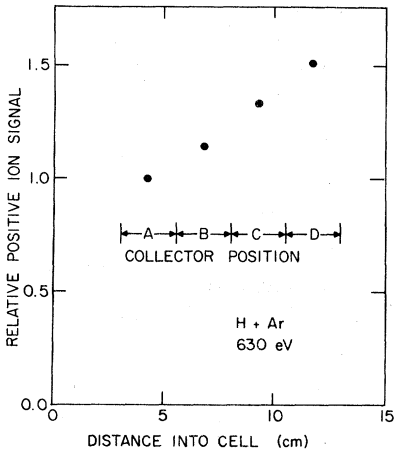

FIG. 2. Relative positive ion signal to collectors A, B, C, and D as a function of their distance into the target cell.

It was soon realized that the increased signal recorded at those collectors located deeper into the target cell is due to arrival of fast protons that have been scattered through large angles during their collisional formation within the cell. This scattered proton signal is superimposed on a position-independent (and therefore collector-independent) signal corresponding to the rate of production of slow Ar^+ ions.[23] Thus the total measured signal to the ith collector S^+_{mi} is given by

$$S^+_{mi}=S_{Ar^+}+BN\int_0^X\left(\int_{\Delta\Omega_i(x,\theta,\phi,V)}F(x,\theta)\frac{d\sigma_{01}}{d\Omega}\,d\Omega\right)dx\,, \tag{7}$$

where S_{Ar^+} is the desired Ar^+ signal, $d\sigma_{01}/d\Omega$ is the differential proton production cross section, and B and N are as defined earlier. Here dx is an element of length along the neutral beam cell axis (of total length X) from which a proton, scattered at angle θ and azimuth ϕ, and into the range of solid angle $\Delta\Omega_i(x,\theta,\phi,V)$, may reach the ith collector surface under the influence of target-cell potentials V. The experimental factor $F(x,\theta)$ accounts for the target gas density gradient near the cell entrance ($x=0$) and certain geometrical limitations preventing scattered protons produced near the cell entrance from reaching the collector stations (see the entrance configuration of the cell in Fig. 1).

If S_{Ar^+} is to be determined from the measured S^+_{mi}, the second term on the right of Eq. (7) must be evaluated. While computation of the orbits of all scattered protons under the influence of cell potentials V is tedious, the limiting factor in the evaluation is a lack of knowledge of $d\sigma_{01}/d\Omega$.

On the other hand, if only the angular dependence

of $d\sigma_{01}/d\Omega$ were known (as opposed to its absolute value as well), the problem becomes tractable. If the measured signals to collectors B and C, for example, are written as

$$S^+_{mB} = S_{Ar^+} + S^+_{pB}, \tag{8}$$

$$S^+_{mC} = S_{Ar^+} + S^+_{pC} = S_{Ar^+} + K_{CB} S^+_{pB}, \tag{9}$$

where S^+_{pB} and S^+_{pC} are the scattered proton signals to collectors B and C [nothing more than the last term of Eq. (7) evaluated for these collectors], the scattered proton signal to collector C can be related to that to collector B by the parameter K_{CB}, where

$$K_{CB} = \frac{S^+_{pC}}{S^+_{pB}} = \frac{\int_0^X \left[\int_{\Delta\Omega_C(x,\theta,\phi,V)} F(x,\theta)(d\sigma_{01}/d\Omega)\, d\Omega\right] dx}{\int_0^X \left[\int_{\Delta\Omega_B(x,\theta,\phi,V)} F(x,\theta)(d\sigma_{01}/d\Omega)\, d\Omega\right] dx}. \tag{10}$$

Since $d\sigma_{01}/d\Omega$ appears in both the numerator and denominator of Eq. (10), its absolute value is not required in order to determine K_{CB}. Consequently, if its dependence upon θ could be determined, K_{CB} could be evaluated. Using the measured S^+_{mB} and S^+_{mC} values and the computed K_{CB}, Eqs. (8) and (9) can be solved for their two unknowns, S_{Ar^+} and S^+_{pB}.

Parameters K_{AB} and K_{DB} can be similarly computed, yielding four equations with the same two unknowns. Solving these in various combinations gives six separate values of S_{Ar^+} and S^+_{pB}. If the six values agree to within reasonable uncertainty, this constitutes a check on the angular dependence of $d\sigma_{01}/d\Omega$ used in the analysis, for these independent results are composed of scattered proton signals spanning rather different ranges of scattering angle θ. In addition, once the value of S^+_{pB} is available, the absolute value of $d\sigma_{01}/d\Omega$ can be determined by normalization of its angularly dependent form to satisfy Eq. (7).

The angular dependence of $d\sigma_{01}/d\Omega$ has been calculated theoretically under the assumption that it is comparable to $d\sigma_e/d\Omega$, the differential cross section for elastic scattering in H+Ar collisions. While the reader may, and in fact should, question the validity of this assumption, it should be stressed that the scattering angles involved here are generally large. To produce such large-angle scattering, a rather violent small-impact-parameter collision is required, at least at energies in excess of 300 eV or so. Thus the proton nucleus of the incident hydrogen atom must penetrate rather deeply into the electron cloud of the Ar atom. As a result of this rather strong encounter, it is unlikely that the post-collision orbit of the scattered particle will exhibit a strong dependence on whether the particle leaves the collision as a hydrogen atom or proton. Of course, this argument is not really valid in the 100-eV region, as an effective Z value of only a few charge units is all that is required to produce substantial scattering. As will be presently discussed, however, only collectors A and B can be used in any case in this low-energy region. Except at the lowest energy of 50 eV, where the target-cell potentials are sufficient to drive even forward scattered protons to collector B, rather large scattering angles (~30°) are required to reach these collectors, thus still demanding rather hard collisions. The validity of the assumption that the angular dependences of $d\sigma_{01}/d\Omega$ and $d\sigma_e/d\Omega$ are similar is taken up in more detail in paper II.

As an example of this procedure for determining σ_{Ar^+}, consider once again the data of Fig. 2. If both sides of Eq. (7) are divided by the product NBL, it can be written as

$$\sigma^+_{mi} = \sigma_{Ar^+} + \frac{1}{L}\int_0^X \left(\int_{\Delta\Omega_i(x,\theta,\phi,V)} F(x,\theta)\frac{d\sigma_{01}}{d\Omega}\right) dx. \tag{11}$$

The "apparent measured cross section" σ^+_{mi} for these data are 1.58, 1.80, 2.09, and 2.37 (all times 10^{-17} cm^2) for collectors A, B, C, and D, respectively. Using the computed $K_{AB} = 0.4348$, $K_{CB} = 1.683$, and $K_{DB} = 2.652$, the six possible solutions for the Ar^+ production cross section yield $\sigma_{Ar^+} = 1.44 \times 10^{-17}$ cm$^2 \pm 5.6\%$, where 5.6% is the standard deviation of the determinations. Since much of this variance can be accounted for by uncertainties in the measured data, the close agreement supports the conclusion that the angular form of $d\sigma_{01}/d\Omega$ used in the analysis is not substantially in error.

Attention is now directed to the effects of various target-cell potentials on the measured ion signals. Figures 3 and 4 show the dependence of the positive ion signals as functions of the grid potential V_g and the negative charge collector potential V_{nc}. (In keeping with the philosophy stated earlier of presenting various test data for species other than Ar, the results shown are for N_2 targets at a hydrogen-atom energy of 500 eV.)

Consider first the data of Fig. 3, the measured positive ion signals at collectors A through D as a function of grid potential V_g. Note that at V_g values more negative than about −10 V, the various signals reach plateau values, but rise dramatically at less negative V_g to considerably higher plateaus at positive V_g. This behavior is attributed to secondary electrons leaving the various collector surfaces, with grid potentials less negative than −10 V being insufficient to "trap" the secondaries

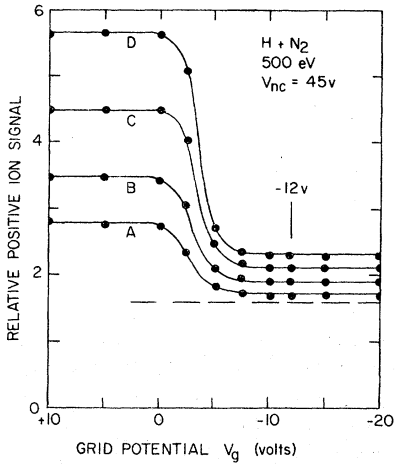

FIG. 3. Relative positive ion signal to collectors A, B, C, and D as a function of the grid potential V_g.

generated by the impact of the fast scattered protons and hydrogen atoms. At positive V_g, all secondary electrons will be accelerated away from the collector surfaces, giving rise to another plateau region.[24] Note that, if provision were not included to evaluate the effects of the secondary electrons and the scattered protons, it would be tempting to assign an $S_{N_2^+}$ signal to the process that would be up to four times larger (depending upon where into the target cell an ion collector were located) than the correct value indicated by the dashed line in Fig. 3.

The data of Fig. 4 show the dependence of the same ion signals on the negative charge collector potential V_{nc}. Note, for example, the curve for collector B. The measured signal rises abruptly with increasing V_{nc} to a "saturation" value at about

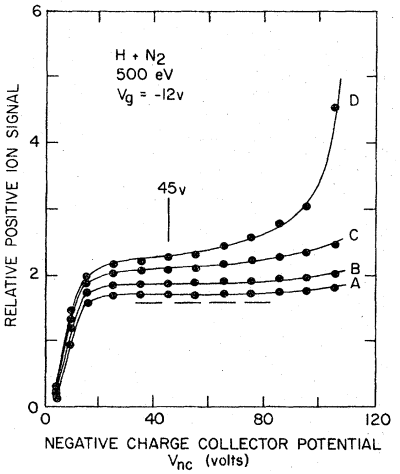

FIG. 4. Relative positive ion signal to collectors A, B, C, and D as a function of the negative charge collector potential V_{nc}.

$V_{nc} \approx 25$ V. This saturation plateau corresponds to essentially a 100% collection efficiency for the slow target ions. The plateau is not totally flat, however, as can be seen by the turning up of the signal again for $V_{nc} \gtrsim 70$ V. This increase results from the influence of the V_{nc} potential on the orbits of scattered protons. Larger V_{nc} values accelerate more scattered protons toward the positive ion collectors, thereby allowing collection of protons with smaller initial scattering angles. Basically similar features are exhibited by the data for collectors A and C. On the other hand, the curve for collector D exhibits only a marginal plateau region. In fact, for $V_{nc} \approx 110$ V, a proton produced near the target-cell entrance and scattered at 0° will reach the rear of collector D under the influence of the applied V_{nc} and V_g.

In principle, this situation should cause no difficulty in our analysis in that the effects of the target-cell potentials on the scattered protons are taken into account. On the other hand, the analysis takes the angular dependence of the differential proton scattering cross section to be the same as that for elastic scattering. While this assumption may be reasonable for large-angle scattering, the elastic $d\sigma_e/d\Omega$ will probably far exceed $d\sigma_{01}/d\Omega$ in magnitude for forward or small-angle scattering. Thus the analysis may be substantially in error if it is applied to a situation where forward or very-small-angle scattered protons are included.

As a result of this problem, the measured results for collector D are omitted for hydrogen-atom energies below 400 eV. A similar situation exists for collector C below 200 eV. In fact, at energies below 80 eV, the data for collector B suffer from a similar difficulty. As the analysis used requires at least two collectors, however, the results for collector B must be kept even though they are rather ambiguous. Fortunately, at least for Ar targets, a competing process essentially negates the importance of scattered protons at these low energies.

One other feature of the target-cell configuration used should be discussed. Namely, if the positive ion collection fields are made sufficiently large, both the slow Ar^+ and the fast H^+ can be completely collected. For collision energies below 1 keV, the total cross section for positive charge production σ_t^+ could thus be determined (above this energy the potentials required caused breakdown in the cell). Of course, σ_t^+ must be identical with σ_t^-, yet to be described. It was comforting to find that these independent measurements, taken under vastly different experimental conditions and typically months apart in time, were indeed the same. In fact, the cross section ratio (σ_t^-/σ_t^+), averaged over the energies below 1 keV, was found to be

$1.001 \pm 3.6\%$ (again, a standard deviation of the ratios), with the largest single discrepancy of 7.3% occurring at 50 eV where, as already and again to be noted, the data include considerable uncertainty. This agreement largely removes major concern over independent evaluation of such otherwise elusive problems as ions bouncing from collector surfaces, substantial secondary ion emission from the surfaces, or improper accounting for various secondary electron phenomena.

Attention is now returned to collection of negatively charged collision products. Here, as was the case for positive ion collection, it was necessary to investigate the effects of the grid potential V_g on the negative charge signals to determine whether the "saturation collection" condition had been reached. It was found that the saturation curves exhibited small structures at grid potentials well in excess of those expected to achieve saturation. As calculations of charged particle orbits within the cell had already become routine, it was soon realized that these structures were occurring at precisely those potentials at which an H^- ion, produced near the cell entrance and forward scattered, would arrive at a collector edge under the influence of the negative V_g. Following the suggestion that the structure present in the σ_t^- cross section for $H+H_2$ collisions might be due to H^- formation,[25] we decided to investigate grid saturation effects with an H_2 target.

One result of this investigation is shown in Fig. 5. Plotted here are the negative charge production signals to collectors F and R (see Fig. 1) as functions of the grid potential V_g. The data are for 250-eV hydrogen-atom energy, for which conditions the H^- formation is substantial (as opposed to the small structures mentioned above).

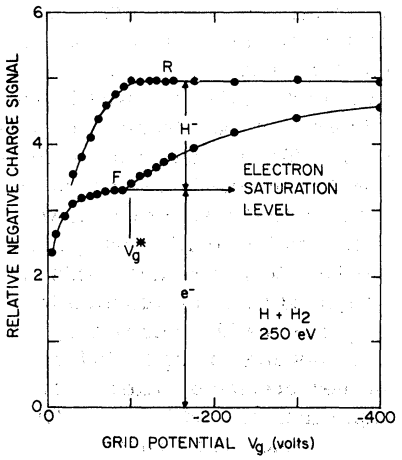

FIG. 5. Relative negative charge signal to collectors F and R as a function of the grid potential V_g.

The authors interpret these results as follows. Simple orbit calculations show that an H^- ion, produced near the cell entrance and forward scattered, will reach the negative charge collector plane at the boundary between collectors F and R if the grid potential is set to −100 V. (This critical value of V_g, labeled V_g^* in Fig. 5 is, of course, energy dependent.) Thus at V_g^*, H^- ions produced along the first 5 cm of the neutral beam path within the target cell should be collected along the 5 cm length of collector R. At more negative V_g, the ions formed very near the cell entrance will begin to be deflected sufficiently to reach the rear of collector F, causing an increase in its recorded signal. Because of the very large deflections required to saturate collector F for H^- ion collection (because of its proximity to the cell entrance), saturation to this collector does not occur until $V_g \approx -1200$ V (not shown in Fig. 5). At this value, the signals to the two collectors are the same.

For V_g values less than V_g^*, on the other hand, forward scattered H^- ions cannot reach collector F. The signal measured to this collector under these conditions is therefore attributed to electrons. At higher collision energies, the electron collection saturation curve (i.e., curve F below −100 V) remains about the same,[26] but exhibits a plateau region before the onset for H^- collection begins.

Thus by measuring the signal to collector R with V_g more negative than V_g^*, the sum of the e^- and H^- signals can be recorded and σ_t^- determined. A value $V_g = 1.2V_g^*$ was used for the measurements reported here. On the other hand, the signal to collector F with $V_g = 0.8V_g^*$ should be composed largely of electrons. The σ_{0-1} cross section therefore can be determined by subtraction of the cross sections measured at the two collectors.

Data at 250 eV were selected for Fig. 5 because this represents a limiting case for separation of the signals for e^- and H^- detection. At lower energies, the electron saturation is not yet achieved for collector F by the time that H^- ions begin arriving. By making the assumption, however, that the electron saturation collection curve remains the same at lower energies, it is still possible to obtain a reasonable estimate of σ_{0-1} by suitably correcting the data for this effect. This problem does not affect the σ_t^- data obtained from collector R.

Looking ahead to the data for Ar targets, it is found that substantial H^- ion formation can again occur. Unfortunately, however, the negative ion contribution does not become large until the incident hydrogen-atom energy is about 100 eV or lower, in which range the separation of the e^- and H^- signals becomes less definitive. In addition, the separation of these signals by the techniques

described assumes that the H^- ions are forward scattered at their formation, as appears to be the case at higher energies. This condition will almost certainly be increasingly violated with decreasing energy and is probably more severe with the heavy Ar targets than with the much lighter H_2 targets.[27] Obviously, if an H^- ion is scattered slightly toward collector F during its formation, it will be counted in with the "electron only" signal, thereby resulting in a reduction of the measured σ_{0-1} cross section. This problem will be discussed in more detail in conjunction with the presentation of the σ_{0-1} results in Sec. V.

The effect of scattered protons on the σ_{Ar^+} measurements described earlier is rather substantial. While the effect of scattered protons on the negative charge collection measurements is much smaller, it cannot be ignored. Thus, large-angle scattered protons can also arrive at the negative charge collectors, this positive current now cancelling a portion of the desired negative charge signal. A relationship similar to Eq. (7) can be written to represent the situation, with the exception that the last term is now negative.

Fortunately, $d\sigma_{01}/d\Omega$ is available from the positive ion studies discussed earlier. As expected, the effect of this correction to the data is to increase the σ_t^- cross section. Once again looking ahead, the authors suggest that this effect is at least partially responsible for the somewhat larger σ_t^- reported here as compared to the results of other investigators.

For every charged particle collection measurement investigated, the various signals were found to be directly proportional to the neutral hydrogen-atom beam intensity. On the other hand, such signals were not always directly proportional to target-cell density. Slight quadratic density dependencies were observed (i.e., the cross section, or signal divided by density, was a function of density). There is little question that these effects are due to multiple scattering phenomena. For example, a hydrogen atom entering the target cell could be elastically scattered through a small angle before being ionization-stripped of its electron in a subsequent collision. For most of the cross-section results presented, the cross-section density dependence rarely exceeded a few percent, but it was rather pronounced for the σ_{0-1} measurements and those phenomena associated with angular proton scattering. To overcome this problem, data were always taken as a function of the target-cell density and a suitable zero-density extrapolation performed. A ±3% uncertainty from this source was assigned to the cross-section values presented here.

The various charged particle signals themselves were assigned an uncertainty of ±5% from such sources as instrument calibrations, nonlinearities, and the statistics associated with the signal measurements. The uncertainties discussed here as well as those placed on the hydrogen beam flux and the density determination discussed in Sec. II are combined with the uncertainties resulting from the data-analysis procedures and presented in tabular form in Sec. IV.

In the course of making the measurements described here, numerous other tests and evaluations of the data were undertaken. For example, by intentionally diverting the entering hydrogen-atom beam to an off-axis angular orientation inside the target cell,[28] the effects of the various scattering phenomena on the measurements could be evaluated. Thus, if the beam were directed slightly towards the positive charge collectors, a slightly smaller scattering angle was required for a proton to reach these collectors, thereby increasing the scattered proton contribution to the positive charge signal. Other tests included the effects of minor defocusing of the entering beam, the effectiveness of the charged-particle trap at the rear of the target cell, and an evaluation of the possibility that charged particles were entering the target cell along with the neutral hydrogen-atom beam. In all cases, the results of imposing these and other perturbations on the normal system operating conditions behaved in a generally predictable way, and were used to verify the appropriate criteria for proper system operation.

IV. σ_t^-, σ_t^+, σ_{Ar^+}, AND σ_{01} RESULTS AND UNCERTAINTIES

The results of the measurements for the σ_t^-, σ_t^+, σ_{Ar^+}, and σ_{01} cross sections are here presented and compared, where possible, with the data of other investigators. The data are presented as graphs of cross sections vs laboratory hydrogen-atom energy. While the present measurements extend only up to an energy of 3 keV, the various plots extend up to 30 keV, so that better comparisons with the results of other workers can be made. The results of the present studies are plotted as solid data points with solid lines through the points, and the results of other investigators are displayed by open symbols and broken curves.

The first data presented, in Fig. 6, are the σ_t^- and σ_t^+ cross-section measurements. The σ_t^- results of Dehmel, Meger, and Fleischmann[29]; McNeal, Clark, and Klingberg[20]; and Solov'ev, Il'in, Oparin, and Fedorenko,[30] are shown for comparison. The present results average about 15% higher than those reported by Dehmel *et al.* (well within the combined uncertainties), and about 40% higher than those reported by McNeal *et al.* (about 15% outside combined uncertainties). While

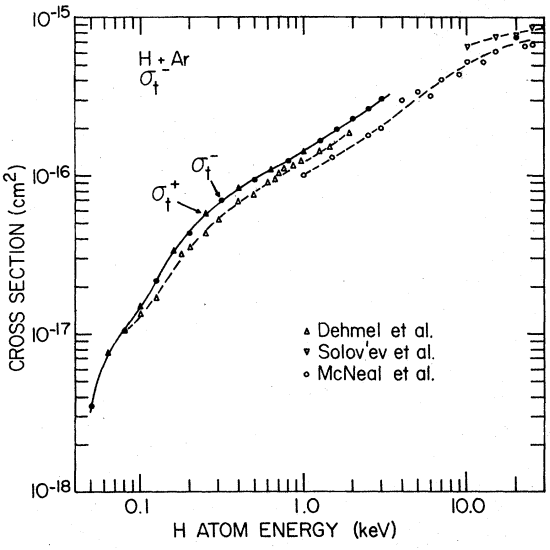

FIG. 6. Total charge production cross sections. Solid circles and triangles are present results. Other data are from McNeal *et al.* (Ref. 20), Dehmel *et al.* (Ref. 29), and Solov'ev *et al.* (Ref. 30).

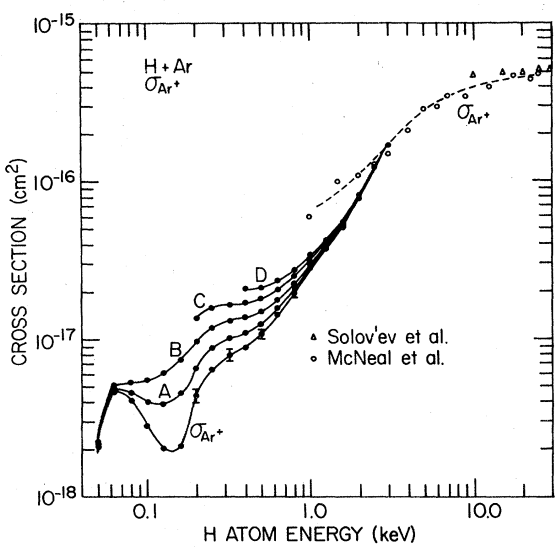

FIG. 7. Measured positive ion cross sections to collectors A, B, C, and D and the Ar^+ production cross sections. Solid circles are present results. Other data are from McNeal *et al.* (Ref. 20) and Solov'ev *et al.* (Ref. 30).

no direct comparison can be made, the present results would appear to agree quite well with those of Solov'ev *et al.*, if a smooth cross-section extrapolation were made across the energy gap between the measurements.

Some fraction of the larger magnitude of the present σ_t^- over those found in the other low-energy investigations can be accounted for, as noted in Sec. III, by the failure of the other investigators to include the effects of protons scattered to their negative charge collectors. As such corrections depend on a detailed knowledge of the grid potential, the target-cell geometry, and the direction and divergence of the hydrogen-atom beams employed, the present authors are in no position to estimate the amount of correction required in these earlier measurements. It seems possible, however, that such corrections would bring the results of all the measurements into agreement within uncertainties.

As noted in Fig. 6, the present data points in the region below 1 keV show alternately the results of the σ_t^- and σ_t^+ measurements. The reader may recall from Sec. III that the root-mean-square deviance of these independent measurements is only ±3.6% on an absolute basis.

Figure 7 shows the "apparent measured cross sections" to collectors A, B, C, and D and the σ_{Ar^+} cross section determined from the procedures outlined in Sec. III. Also shown are the σ_{Ar^+} results of McNeal *et al.*[20] and Solov'ev *et al.*[30]

Note first that the data for collectors A through D are very close in the energy range above 2 keV. The bulk of the observed positive ion signal here is attributed to Ar^+. On the other hand, these measured results begin to diverge substantially with decreasing energy, showing the effect of scattered protons on the various collector signals. As mentioned earlier, to avoid the forward scattering problem for proton production, signals to collectors D and C are discarded below 400 and 200 eV, respectively.

The flags on the σ_{Ar^+} cross section at a few energies represent the standard deviations of the σ_{Ar^+} values obtained from the individual pairs of collectors used for the analysis[31] and should not be taken as absolute uncertainties.

Note the existence of the dominant peak in the σ_{Ar^+} cross section in the 70-eV region. (A close analysis of the σ_t^- data in Fig. 6 reveals a slight "hump" in this energy range.) The present authors attribute this structure to the $H^- + Ar^+$ ion pair formation reaction and will attempt to confirm this assignment when the σ_{0-1} cross-section data are presented in Sec. V. In addition, the existence of a second structure in the 300-eV range is apparent.

The present σ_{Ar^+} results are in good agreement with the data of McNeal *et al.* at 3 keV. Note, however, that the two results diverge rapidly with decreasing energy. The present authors suggest, as noted in Sec. III, that this discrepancy may result from secondary electron effects present in the McNeal *et al.* measurements. As these secondary electrons are caused by the impact of fast

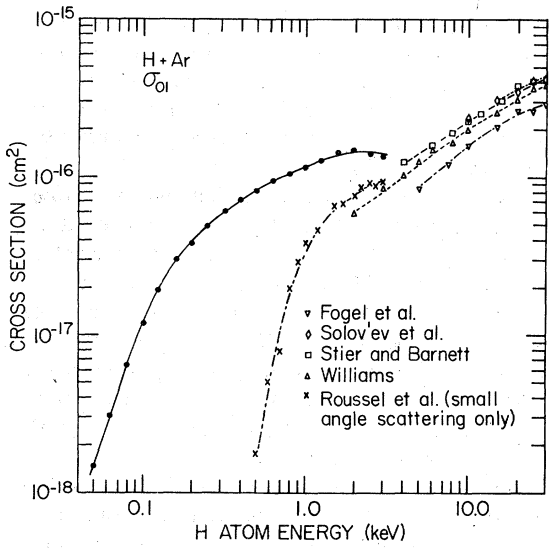

FIG. 8. Proton production cross sections. Solid circles are present results. Other data are from Solov'ev *et al.* (Ref. 30), Fogel *et al.* (Ref. 34), Stier and Barnett (Ref. 33), Williams (Ref. 35), and Roussel *et al.* (Ref. 36) (small-angle scattering only—see text).

elastically scattered hydrogen atoms and inelastically scattered protons to the collector surface, the energy dependence of the problem should go approximately[32] as E^{-1}. Thus if this assignment is correct, the σ_{Ar^+} data of McNeal *et al.* should be largely free of such difficulty at the higher energies.

Attention is now directed to Fig. 8, which depicts various results for the σ_{01} cross section. The present results were obtained by subtracting σ_{Ar^+} from σ_t^-, as indicated by Eq. (4). Other measured σ_{01} results shown include those of Stier and Barnett[33]; Fogel, Ankudinov, Pilipenko, and Topolia[34]; Williams[35]; and Solov'ev *et al.*[30]

Also shown in Fig. 8 are the results of Roussel, Pradel, Schlachter, and Spiess.[36] These data do not represent a total σ_{01} cross section, but rather $d\sigma_{01}/d\Omega$ integrated only over the 0 to 10 mrad acceptance angle of their detector. Thus these investigators would not collect any protons scattered at angles in excess of about 0.6° during their formation.

At first glance, the present results appear to contradict (in both magnitude and energy dependence) the data of the other investigators cited. While the present results and those of Stier and Barnett have comparable magnitudes in the 3 to 4 keV region, the comparison suggests a σ_{01} which exhibits structure in the 1 to 5 keV region. The data of Williams fall well below the present results in the 2 to 3 keV region, as does any extrapolation of the work of Fogel *et al.* In fact, the Williams data agree rather well with the essentially forward scattered proton production results of Roussel *et al.*

Like the experiments of Roussel *et al.*, the experiments of Williams and Fogel *et al.* are "cell transmission" experiments. In all these studies, a hydrogen-atom beam was directed through an Ar target cell whose dimensions were defined by relatively small entrance and exit apertures. Protons (and H^- ions) emerging from the cell were then separated and collected by various detector arrangements.

From the publications of Williams and Fogel *et al.*, it is difficult to determine their detector acceptance angles for proton production. In view, however, of the approximate agreement between their results and those of Roussel *et al.*, it seems probable that only rather forward scattered protons were being detected, at least at the lower energies.

In view of the substantial numbers of protons scattered at angles on the order of 10° or more (see data of Figs. 2 or 7) during their formation, it is apparent that any experiments in which are collected only those protons scattered essentially in the forward direction will grossly underestimate the σ_{01} cross section. In fact, if the present total σ_{01} cross section is compared with the small-angle integrated $d\sigma_{01}/d\Omega$ data of Roussel *et al.*, it appears that on the order of 90% of the protons produced in 700-eV hydrogen-atom collisions with argon are scattered in excess of 0.6° during their formation.

The σ_t^- and σ_{Ar^+} results of McNeal *et al.*[20] can also be used to obtain a σ_{01} cross section. McNeal *et al.* do not present such data, as the uncertainties in their σ_t^- and σ_{Ar^+} measurements prohibit a definitive evaluation. If the evaluation is made, however, the energy dependence of the resulting σ_{01} above about 5 keV is in general agreement with those energy dependences obtained by the other workers cited. On the other hand, in the 1 to 5 keV range, the results are not inconsistent with an approximate plateau region in σ_{01} as indicated by the present data.

In sharp contrast to the disagreement between the various σ_{01} cross sections for argon targets as shown in Fig. 8, a similar comparison for the much lighter H_2 target species indicates essential agreement between the present method for σ_{01} determination and the results from the "cell transmission" measurements. Of course, the effects of angular scattering are far smaller for this light low-Z target. In addition, a pronounced structure in the σ_{01} cross section for this target in the 1 to 5 keV region is apparent,[37] similar to what would be obtained if the present σ_{01} cross section for argon targets is joined smoothly onto the results of Stier and Barnett in the 3 to 4 keV

region (see Fig. 8).

Smith, Duncan, Geis, and Rundel[8] have recently made measurements of σ_{01} cross sections for hydrogen-atom collisions with molecular targets including N_2, O_2, CO, and CO_2.[38] While these workers did not investigate Ar targets, their results for these heavier molecules are not strongly species dependent, and the σ_{01} cross sections all have a shape and magnitude rather similar to the present σ_{01} results for Ar targets. (The present σ_{01} cross sections for N_2 and O_2 targets are also somewhat in conflict with the results of Smith *et al.*, but the discrepancies are considerably smaller than those found for Ar targets, as shown in Fig. 8.)

The uncertainties in the σ_t^-, σ_{Ar^+}, and σ_{01} cross sections presented here are listed in Table I along with the cross-section values themselves. These total uncertainties incorporate the uncertainties in the measurement of the various experimental parameters required for the cross-section determinations, an estimate of the degree to which various spurious phenomena could be contributing to the measurements, and an approximate evaluation of the uncertainties that result from the data-analysis procedures employed.

The basic uncertainties present in the measurements of the various experimental parameters required for the cross-section determinations have already been listed in earlier sections. Quadrature combination of these individual uncertainties[39] and an additional ±7% resulting from the authors's inability to determine that the measured signals are free from erroneous contributions (secondary electrons and ions, bouncing ions, etc.) to below this level, yield a ±11% net uncertainty. At the lowest hydrogen-atom energies, this net uncertainty is increased to ±13% at 80 eV, ±15% at 63 eV, and ±20% at 50 eV, to account for the less well-defined hydrogen-atom beam diameter and collinearity properties and the somewhat larger quadratic density dependencies of the measured signals found here. These uncertainties are standard in the sense that they are applied to all the measured cross sections. The authors know of no other uncertainties that might affect the σ_t^- cross-section measurement.

TABLE I. Cross sections and total uncertainties as a function of hydrogen-atom energy.

H-atom energy (eV)	Cross sections (10^{-16} cm^2) and total uncertainties σ_t^-	σ_{Ar^+}	σ_{01}
3000	3.04 ± 11%	1.70 ± 11%	1.34 ± 29%
2500	2.64 ± 11%	1.24 ± 11%	1.40 ± 23%
2000	2.29 ± 11%	0.782 ± 12%	1.51 ± 18%
1600	1.96 ± 11%	0.511 ± 12%	1.45 ± 16%
1250	1.66 ± 11%	0.373 ± 13%	1.29 ± 15%
1000	1.44 ± 11%	0.280 ± 14%	1.16 ± 14%
800	1.25 ± 11%	0.196 ± 15%	1.05 ± 14%
630	1.08 ± 11%	0.144 ± 16%	0.940 ± 13%
500	0.939 ± 11%	0.109 ± 17%	0.830 ± 13%
400	0.812 ± 11%	0.0900 ± 18%	0.712 ± 13%
320	0.690 ± 11%	0.0827 ± 19%	0.607 ± 13%
250	0.550 ± 11%	0.0636 ± 20%	0.486 ± 13%
200	0.387 ± 11%	0.0443 ± 22%	0.387 ± 13%
160	0.320 ± 11%	0.0210 ± 23%	0.229 ± 12%
125	0.216 ± 11%	0.0202 ± 23%	0.196 ± 12%
100	0.147 ± 11%	0.0280 ± 21%	0.119 ± 14%
80	0.106 ± 13%	0.0412 ± 20%	0.0643 ± 25%
63	0.0780 ± 15%	0.0471 ± 20%	0.0310 ± 48%
50	0.0348 ± 20%	0.0201 ± 22%	0.0147 ± 56%

The σ_{Ar^+} results suffer from the above standard uncertainties as well as those arising from removal of the effects of scattered protons on the measurements by the techniques described. At energies of 200 eV and above, three or more σ_{Ar^+} values were obtained by applying the data-analysis procedures to various pairs of the positive ion collectors, and standard deviations for the determinations were computed.[31] A plot of these standard deviation values against the logarithm of the hydrogen-atom energy yields an approximately straight line of negative slope having value of ±9% at 200 eV and diminishing to ±2% at 3 keV. Considered as an ensemble, about 7% of the total number of individual σ_{Ar^+} determinations fell outside their respective "two times the standard deviation" limits, as compared to the figure of about 10% which would be expected from a large random sample. The authors thus concluded that uncertainties of twice the value found from the standard deviation vs $\log_{10}E$ plot would provide approximately 90% confidence limits for the results.

Of course, this procedure could not be extended to below 200-eV hydrogen-atom energy, as only collectors A and B were used here to determine a single σ_{Ar^+} value. Uncertainties in this region were obtained simply by extrapolating the standard deviation vs $\log_{10}E$ plot into this region and again taking twice the extrapolated standard deviation values. As can be seen from Fig. 7, however, the effects of the protons scattered to these collectors in the region below 100 eV become smaller, because the $H^- + Ar^+$ pair production is the dominant contributor to the positive ion signal in this region. The uncertainty in the σ_{Ar^+} cross section from the scattered proton source was thus reduced from the extrapolated maximum value of ±20% at 125 eV to ±10% at 50 eV.

In the above uncertainty analysis, it has been assumed that the uncertainties in the various σ_{Ar^+} determinations are purely statistical. As men-

tioned in Sec. III, however, an incorrect assumption on the angular dependence of $d\sigma_{01}/d\Omega$ will also give rise to differing σ_{Ar^+} values as derived from different combinations of the positive ion collectors used. In general, it is not expected that the statistical functuations in the individual σ_{Ar^+} values from measurement of the various positive ion signals should exceed about ±5%. Thus at energies below about 500 eV, the somewhat larger standard deviations exhibited by the σ_{Ar^+} results appear to indicate that the angular dependencies of the required $d\sigma_{01}/d\Omega$ and the assumed $d\sigma_e/d\Omega$ are beginning to differ.[40] However, as the differences in the σ_{Ar^+} values obtained from the various collector pairs from this source are included in the "standard-deviation-related" uncertaintity already specified, no additional uncertainty increase is made.

The uncertainty in the σ_{Ar^+} cross section resulting from the effect of scattered protons is combined in quadrature with the standard uncertainty associated with the measurements themselves to obtain the net uncertainty assignment for the σ_{Ar^+} results. The results are given in the third column of Table I.

Because the σ_{01} cross section is determined by subtracting the σ_{Ar^+} cross section from the σ_i^- results, the uncertainties in σ_{01} are given by

$$\delta\sigma_{01} = [(\delta\sigma_{Ar^+})^2 + (\delta\sigma_i^-)^2]^{1/2}. \quad (12)$$

The results of this uncertainty evaluation are listed in the fourth column of Table I. In fact, these results are probably overestimates of the true uncertainties, as the systematic uncertainties have been included twice. However, as the σ_i^- and σ_{Ar^+} results were obtained at rather different times during the total measurement program, the σ_{01} uncertainties were assumed to be given by Eq. (12).

V. $H^- + Ar^+$ ION PAIR FORMATION REACTION

The final results to be presented are those for σ_{0-1}, shown in Fig. 9 together with the work of Stier and Barnett,[33] Fogel *et al.*,[34] and Williams.[35] Also shown are the small-angle integrated $d\sigma_{0-1}/d\Omega$ results of Roussel *et al.*,[36] obtained with the same techniques as used for looking at proton production.

The cross-section data presented in Sec. IV are of high quality from the viewpoint of minimum uncertainty, high reproducibility, and satisfaction of all the checks and tests to which they were subjected. In sharp contrast, the σ_{0-1} results are not up to these standards. Nevertheless, the measurements were made and their results are presented here because they can be used to interpret

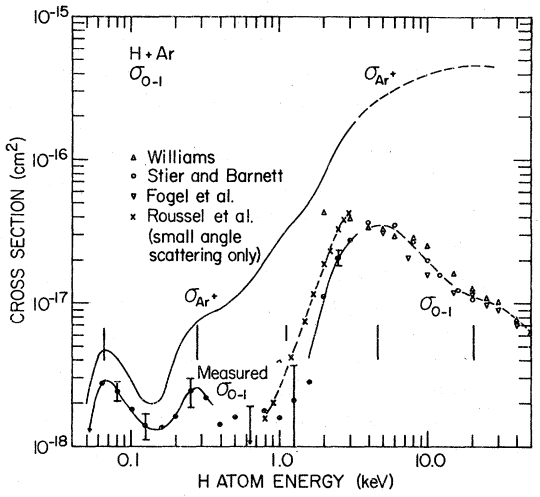

FIG. 9. H^- production cross sections. Solid circles are present results. Other data are from Stier and Barnett (Ref. 33), Fogel *et al.* (Ref. 34), Williams (Ref. 35), and Roussel *et al.* (Ref. 36) (small-angle scattering only—see text). The σ_{Ar^+} data of Fig. 7 are shown for comparison.

structures present in the σ_{Ar^+} cross section, which is also included in Fig. 9. The results also illustrate some rather interesting aspects of the basic $H^- + Ar^+$ ion pair formation reaction.

Note the existence, once again, of the dominant low-energy peak and the presence of a second such peak in the 300-eV region. The omission of a curve through the present data points in the region between about 350 eV and 1.5 keV denotes an inability to describe the cross-section shape in this energy region. (The reader may recall that these data are basically obtained by subtraction of the negative charge signals to collectors F and R. When the magnitudes of these signals are of order 50 to 100 times their difference, the subtraction obviously becomes dubious.) Above 1.5 keV, however, the data clearly indicate a rapid rise in the cross section with increasing energy.

The flags shown on some of the data points are estimates of the typical upper-limit relative uncertainties present in the measurements and by no means imply absolute uncertainty limits.

With the exception of the 2-keV data point of Williams, the present σ_{0-1} cross section blends in rather smoothly with the higher-energy results of the other workers cited above. The present results also exhibit an energy dependence very similar to that found by Roussel *et al.* for basically forward scattered H^- formation and have a magnitude about $\frac{2}{3}$ as large as the Roussel *et al.* data in the 2 to 3 keV region.

Unfortunately, the procedure employed for determining the present σ_{0-1} cross section also

suffers from the difficulty that the assumption is made that the product H^- ions are forward scattered (see discussion in Sec. III). Both the present results and those of Roussel *et al.* suffer from this problem.[41] As noted earlier,[27] however, $d\sigma_{0-1}/d\Omega$ is much more strongly forward peaked than its $d\sigma_{01}/d\Omega$ counterpart in the 2-keV energy range. Thus the forward scattered H^- formation rate should agree much more closely with the total σ_{0-1} than is the case for proton production in this energy region. The authors thus conclude that the true σ_{0-1} drops rapidly with energy in the 3 to 1 keV region.[42] Furthermore, as present results are uncertain by about a factor of 2 above 2 keV (most considerations suggest that the measured results are low), the present data and those of Roussel *et al.* may be considered to be in approximate agreement.

While the angular scattering of the product H^- will probably not be severe in the 1-keV energy region, the assumption that the H^- will be forward scattered at the lower energies will almost certainly be increasingly violated with decreasing energy. While "curve fitting" may be risky here, it is interesting to speculate that the entire low-energy peak in the σ_{Ar^+} cross section is due to the ion pair formation reaction, and to ask how much the measured σ_{0-1} would have to be increased to make it agree with σ_{Ar^+} in this region. Such an exercise was undertaken, and it was found that if the true σ_{0-1} cross section could be determined from the relationship

$$\sigma_{0-1}(\text{true}) = \sigma_{0-1}(\text{measured})[1 + 50/E], \qquad (13)$$

where E is the hydrogen-atom energy in eV, a rather interesting result was obtained. Not only does σ_{0-1}(true) fall very close to σ_{Ar^+} in the region below 100 eV, but the difference between the two cross sections, $\sigma_{Ar^+} - \sigma_{0-1}$(true), which should be the cross section for simple argon ionization (reaction 2), becomes a smoothly decreasing function of energy in the region below about 600 eV. In other words, both the low-energy peak and the structure in σ_{Ar^+} in the 300 eV region disappear to within the limits of measurement scatter.

The form of Eq. (13), i.e., the E^{-1} dependence of the "correction factor," was not chosen at random. Rather, the authors have found that this form is approximately successful in treating the scattered proton problem at higher energies. While this fact does not necessarily justify application of this form of correction to the σ_{0-1}(measured) results, it is not inconsistent with what might be reasonably expected in terms of its gross features. Thus, even though definitive experimental verification is lacking, the author feels comfortable in concluding that the lower energy structures in the σ_{Ar^+} cross section result from the $H^- + Ar^+$ ion pair formation process.

VI. DISCUSSTION OF THE RESULTS

It is probable that an interpretation of the structures in the cross sections presented here will depend on the details of the collision process. Fortunately, a sufficient number of potential energy curves are available to begin to make some constructive comments concerning the various reaction mechanisms which may occur in H+Ar collisions. A set of such curves is shown in Fig. 10.

The solid curves for the H+Ar, H^++Ar, and H+Ar^+ states of the system were obtained from the calculations of Kuntz and Roach.[43] The ground-state curve is in reasonable agreement with that obtained by the scattering measurements of Mason and Vanderslice[44] in the $1.3 < R < 3.0$ Å region. The H^++Ar curve (exhibiting a well of depth 4.0 eV at 1.38 Å separation) is in good agreement with the scattering results and analysis of Rich, Bobbio, Champion, and Doverspike,[45] who obtain a similarly shaped well of 4.2 eV depth at 1.25 Å separation.

The long-dashed curves leading to the H*+Ar and H+Ar* states at large separations (the $n = 2$ levels of H and the lowest ^3P and ^1P levels of Ar) are rough estimates drawn by the present authors as examples of how such curves might appear.

The short-dashed curve represents an estimate, also by the present authors, made to illustrate the gross features of the $H^- + Ar^+$ interaction energy. This curve was taken to be basically similar to the $H^- + H^+$ curve (the $1s\sigma$, $2p\sigma$, $B^1\Sigma_u^+$ bound state of H_2), and the $H^- + He^+$ curve computed by Ross and Mason.[46] To allow for the somewhat larger

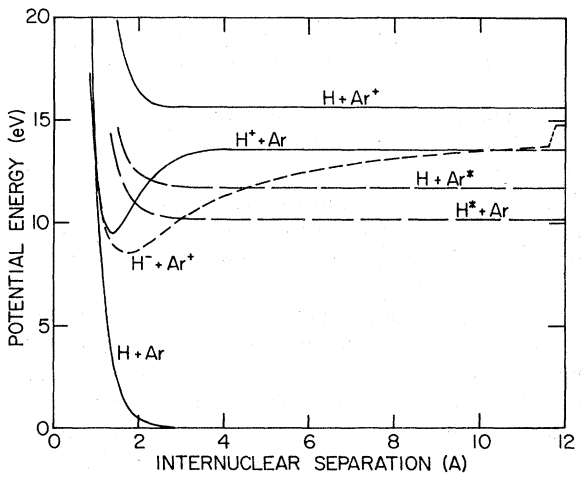

FIG. 10. Approximate potential-energy curves for the H+Ar system.

extent of the Ar^+ ion, as compared to H^+ and He^+, the broad minimum characteristic of such ionic curves was taken to occur at 1.8 Å.[47]

While the detailed shape of the $H^- + Ar^+$ curve in the region inside 2 Å separation is only approximate, it is consistent with a rough calculation made by Olson[42] which indicates that this ionic curve intersects (diabatically) with the ground-state H + Ar curve at about 0.96 Å. The $H^+ + Ar$ curve also crosses the ground-state curve at 0.96 Å. Thus these two crossings, at a potential energy of about 14 eV, are almost certainly the first encountered by an approaching H + Ar pair. As such, the outgoing $H^+ + Ar$ and $H^- + Ar^+$ channels should play an important role in the determination of collision products.

If, during a lower energy H + Ar encounter at small separation, an electron is given sufficient momentum to escape the vicinity of the collision in a time short compared to the time scale of the nuclear motion, the system will probably separate into the $H^+ + Ar$ state. As such, the separating system can cross the $H^* + Ar$ and $H + Ar^*$ system states, with the total-charge inequality preventing transitions at their respective crossing radii.

On the other hand, if the electron is not ejected, the collision products may separate along the $H^- + Ar^+$ channel. During the separation, however, this state must diabatically cross all possible $H^* + Ar$ levels, many of the $H + Ar^*$ levels, and the $H^+ + Ar$ ionization continuum. The probability that the outgoing $H^- + Ar^+$ system will survive such crossings will depend upon the matrix elements of the interaction in the vicinity of the various crossings and the collision velocity.

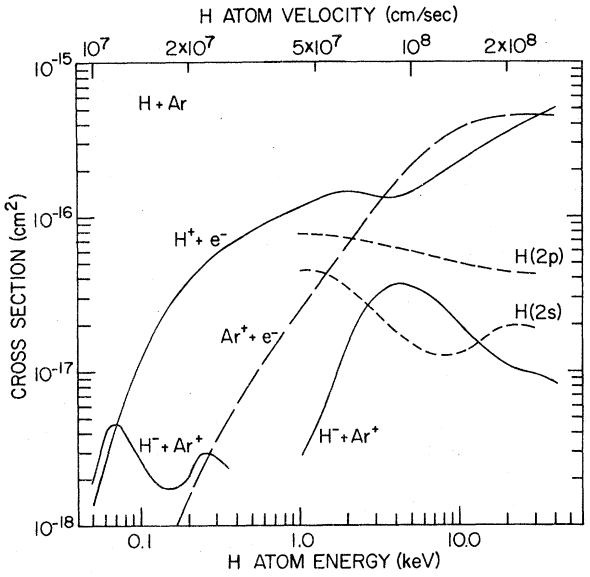

FIG. 11. Charge production and hydrogen-atom excitation cross sections. The dashed curves are from Birely and McNeal (Ref. 48).

The above comments appear to be consistent with the cross-section data presented in Fig. 11. The curve labeled $H^+ + e^-$ is a combination of the lower-energy σ_{01} cross section determined here blended smoothly into the higher-energy results of Stier and Barnett.[33] The curve labeled $H^- + Ar^+$ is the present roughly corrected σ_{0-1}(true) result [see Eq. (13)] in the region below 350 eV. This curve between 1 and 3 keV in an average of the present σ_{0-1} results and those of Roussel *et al.*,[36] and is drawn to merge into the higher-energy results of the other workers cited in Fig. 9.

The curve labeled $Ar^+ + e^-$ represents the cross section for simple Ar ionization and is obtained by subtraction of the $H^- + Ar^+$ cross section shown in Fig. 11 from the σ_{Ar^+} data of Fig. 7. Also included are the cross sections for population of the 2*s* and 2*p* levels of the hydrogen atom in H + Ar collisions as determined by Birely and McNeal.[48]

Note first that the $H^+ + e^-$ production cross section is much larger than its $Ar^+ + e^-$ counterpart at the lower energies. This would appear consistent with the fact that a low-potential-energy crossing to the $H^+ + Ar$ state is available to the interacting system.

Of more interest here, however, is the energy dependence of the $H^- + Ar^+$ cross section. As seen in Fig. 11, this cross section at the higher energies is increasing with decreasing energy. However, it begins to decrease rather abruptly at about 4 keV ($v_H \lesssim 10^8$ cm/sec).

Note that this decrease appears to be accompanied by a marked increase in the H(2*s*) formation cross section. While definitive proof is not available, this observation is consistent with the idea that the outgoing $H^- + Ar^+$ channel is no longer always able to survive its crossing with this $H^* + Ar$ curve, and is therefore feeding this channel. The H(2*p*) cross section is also increasing with decreasing energy in this energy range.[49]

Finally, the $H^+ + e^-$ cross section exhibits a structure at about the same velocity at which the $H^- + Ar^+$ cross section begins to decrease abruptly. The authors are hesitant in attributing this structure to an $H^- + Ar^+ \rightarrow H^+ + Ar + e^-$ transition, because this crossing occurs way out at about 10 Å separation. On the other hand, the H^- ion should be highly polarized as the ionic collision products separate, with its two electrons tending to be concentrated in the region between the separating proton and the Ar^+ ion (in a wave function similar to a stretched but still bound H_2 molecule). When the separation has reached a point above the $H^+ + Ar$ ionization continuum, the tenuous ionic bond may "snap" in a sort of Auger autoionization like process, leaving the remaining bound electron on

the Ar^+ core.

The structure in the $H^- + Ar^+$ cross section at the low energies is in itself of interest. Olson[50] has shown that if the difference between potential energy curves for two crossing states of a system goes through an extremum at an internuclear separation inside a crossing, it is possible to obtain oscillations superimposed on the general velocity dependence of an inelastic total cross section. Such a situation may in fact occur for the $H^- + Ar^+$ and H+Ar curves shown in Fig. 10. There do appear to be four distinct structures in the σ_{0-1} cross section presented in Fig. 9, as indicated by the four tall vertical lines. These four lines, and the shorter line at about 1100 eV, indicate the positions at which structures might be expected if each occurred at twice the velocity of the previous one. While the existence of a structure at 1100 eV cannot be established by the present data, its "predicted location" is close to the 1-keV data point of Roussel *et al.*,[36] which lies well above any smooth curve fitted through the remainder of their data points.

Even if the structures in the σ_{0-1} cross section cannot be attributed to the mechanism proposed by Olson, their regularity may result from some sort of quantum-mechanical phase-interference phenomenon. Similar such structures, although not quite so pronounced or regular, appear in the σ_{0-1} cross sections for most of the other target species studied in these investigations.

We conclude that ion pair formation may represent an important intermediate mechanism in many low-energy neutral-neutral scattering processes. (In fact, such ionic states may be present and contribute to reactions even if neither of the reactants forms stable negative ions at infinite separation.) Thus, any theoretical treatment of such collisions must be considered incomplete if provision for this mechanism is not included.

---

*Supported by the Atmospheric Sciences Section of the National Science Foundation under Grant No. DES73-00654.

[1]For summaries of the history of auroral investigations, see S. Chapman, *Aurora and Airglow*, edited by B. M. McCormac (Reinhold, New York, 1967); or *Atmospheric Emissions*, edited by B. M. McCormac and A. Omholt (Van Nostrand, New York, 1969).

[2]L. Vegard, Nature 144, 1089 (1939).

[3]L. Vegard, *Reports of the Gassiot Committee* (The Physical Society, London, 1948), p. 82.

[4]Numerous publications support this generalization. See, for example, A. Omholt, *The Optical Aurora*, edited by J. G. Roederer and J. Zähringer (Springer-Verlag, Berlin, 1971); or R. H. Eather, Rev. Geophys. 5, 207 (1967).

[5]D. R. Bates, Ann. Geophys. 11, 253 (1955).

[6]R. J. McNeal and J. H. Birely, Rev. Geophys. Space Phys. 11, 633 (1973).

[7]D. W. Koopman, Phys. Rev. 166, 57 (1968); R. J. McNeal and D. C. Clark, J. Geophys. Res. 74, 5065 (1965); F. J. deHeer, J. Schutten, and H. Moustafa, Physica 32, 1766 (1966); R. F. Stebbings, A. C. H. Smith, and H. Ehrhardt, J. Geophys. Res. 69, 2349 (1964). The above listing is only partially complete.

[8]K. A. Smith, M. D. Duncan, M. W. Geis, and R. D. Rundel, J. Geophys. Res. 81, 2231 (1976).

[9]Multiple ionization effects are probably not large at the low collision energies employed here and should thereby have minimal effect on the measurement outcome.

[10]R. J. McNeal and D. C. Clark, J. Geophys. Res. 74, 5065 (1969).

[11]Space-charge effects increased the beam diameter to 2 or 3 mm at energies below 100 eV.

[12]In general, the photodetachment efficiency has an inverse velocity dependence.

[13]B. Van Zyl, N. G. Utterback, and R. C. Amme, Rev. Sci. Instrum. 47, 814 (1976).

[14]For evaluating the uncertainties in the parameters of Eq. (5), the authors treat systematic uncertainties (instrument calibrations, etc.) and statistical uncertainties (meter readings, etc.) as random. The quoted net uncertainty (i.e., ±3% for the beam flux measurements) is obtained by quadrature combination of the individual uncertainties and is estimated to be "on a par" with 90% or higher confidence limits for the measurements.

[15]S. Ruthberg, J. Vac. Sci, Technol. 6, 401 (1969).

[16]MKS Baratron, type 90.

[17]B. Van Zyl, Rev. Sci. Instrum. 47, 1214 (1976).

[18]N. G. Utterback and G. H. Miller, Phys. Rev. 124, 1477 (1961).

[19]Secondary electrons from the grid (99.4% optical transparency at normal incidence) were observed and corrected for. Their contributions to the measured signals was typically on the order of 2%. Nevertheless, a ±2% uncertainty was allowed from this source. Numerous other similarly small sources of erroneous signal were evaluated and, where necessary, corrected for. Space limitations simply do not allow discussion of all these fine details.

[20]R. J. McNeal, D. C. Clark, and R. A. Klingberg, Phys. Rev. A 2, 131 (1970).

[21]This comparison was actually made for N_2 targets. However, the discrepancy between the present results and those given in Ref. 20 (see Fig. 7 in Sec. IV) is very comparable for Ar and N_2 targets.

[22]Simple estimates of the grid transmission for the positive ions as a function of approach angle gave an effective transmission of 98.8%. A correction to the data was made.

[23]The "thin-target" approximation is applied here and appears justified, as the target-cell pressure did not exceed 4×10^{-4} Torr.

[24]The shape of these curves suggests that most of the secondary electrons have energies in the 2 to 5 eV

range.

[25]Suggested by C. F. Barnett to B. Van Zyl (private communication).

[26]In general, for most target species, a grid potential of about −100 V was found sufficient to collect the product electrons. Taking this potential and the target-cell geometry into account, it appears that most of the product electrons have energies below a few tens of eV.

[27]H. H. Fleischmann, C. F. Barnett, and J. A. Ray, Phys. Rev. A 10, 569 (1974). These authors report that the differential cross section $(d\sigma_{0,-1}/d\Omega)$ for H^- formation is far more forward peaked than that for proton production in the 2-keV energy range. However, the $H^- + Ar^+$ formation reaction is rather inelastic, and the transition to this state probably occurs at small internuclear separation, giving rise to substantial angular scattering at the lower energies.

[28]Such diversion was, of course, accomplished prior to the H^- neutralization and was restricted in angle by the 5-mm-diam target-cell entrance apertures.

[29]R. C. Dehmel, R. Meger, and H. H. Fleischmann, J. Chem. Phys. 58, 5111 (1973).

[30]E. S. Solov'ev, R. N. Il'in, V. A. Oparin, and N. V. Fedorenko, Zh. Eksp. Teor. Fiz. 42, 659 (1962) [Sov. Phys.-JETP 15, 459 (1962)].

[31]For the flags shown at 200 and 320 eV, "standard deviations" were computed even though only three separate σ_{Ar^+} values were available.

[32]A plot of the "composite proton scattering cross section" to collector B is shown in Fig. 4 of the following paper. Also shown there is a plot of the "composite hydrogen-atom scattering cross section" as obtained from the scattering calculations described. At energies in excess of 1 keV or so, both of these cross sections exhibit an energy dependence of approximately $1/E$. The situation in the McNeal *et al.* experiment is probably rather similar.

[33]P. M. Stier and C. F. Barnett, Phys. Rev. 103, 896 (1956).

[34]Ia. M. Fogel, V. A. Ankudinov, D. V. Pilipenko, and N. V. Topolia, Zh. Eksp. Teor. Fiz. 34, 579 (1958) [Sov. Phys.—JETP 7, 400 (1958)].

[35]J. F. Williams, Phys. Rev. 153, 116 (1967).

[36]F. Roussel, P. Pradel, A. S. Schlachter, and G. Spiess, in *Electronic and Atomic Collisions*, edited by J. S. Risley and R. Geballe (Univ. of Washington Press, Seattle, 1975), Vol. 1, p. 27.

[37]See, for example, Fig. 4 of Ref. 35.

[38]These measurements were also of the "cell transmission" type but provision was made to accept protons scattered at angles up to 17°.

[39]We are unable to think of any reason for such uncertainties to be interdependent.

[40]Even at 200 eV, however, the lowest energy for which such standard deviations were computed, the value was only ±11%. Thus even here it appears that the relative angular dependences of the two differential cross sections are not excessively different in the angular range considered.

[41]An "angular acceptance" criterion is difficult to establish for the present results, as it depends on ϕ, the azimuthal scattering angle. Small θ (polar angle) scattering in the plane of Fig. 1 would tend to reduce the present $\sigma_{0,-1}$. On the other hand, substantial scattering at right angles to the plane can be tolerated.

[42]R. E. Olson, private communication. Olson has made approximate calculations of $\sigma_{0,-1}$ between 0.1 and 3 keV. His results, in fair agreement with the measurements above 2 keV, also indicate a rapid fall-off of $\sigma_{0,-1}$ with energy below 2 keV, although not as sharp as suggested by the measurements. These computed values fall well below the present measurements below 200 eV and exhibit no structure. While data are not presented, this reaction is discussed in R. E. Olson, Nucl. Instrum. Methods 126, 467 (1975).

[43]P. J. Kuntz and A. C. Roach, J. Chem. Soc. Faraday Trans. II 68, 259 (1972).

[44]E. A. Mason and J. T. Vanderslice, J. Chem. Phys. 28, 1071 (1958).

[45]W. G. Rich, S. M. Bobbio, R. L. Champion, and L. C. Doverspike, Phys. Rev. A 4, 2253 (1971).

[46]J. Ross and E. A. Mason, Astrophys. J. 124, 485 (1956).

[47]The $H^- + H^+$ well minimum occurs at 1.3 Å and that for $H^- + He^+$ at 1.5 Å. Many other "basically ionic" curves have minima in this region (e.g., LiH at 1.6 Å and NaH at 1.9 Å) and are typically about 6.5 eV deep.

[48]J. H. Birely and R. J. McNeal, Phys. Rev. A 5, 257 (1972). The results of other workers are also presented here.

[49]The H(2*p*) cross section shown is actually that for Lyman-α emission. As the 2*p* level will be fed by cascade from higher *ns* and *nd* levels, this cross section may represent transitions at many such crossings.

[50]R. E. Olson, Phys. Rev. A 2, 121 (1970).